Journal of Catalysis **197,** 200–209 (2001)
doi:10.1006/jcat.2000.3085, available online at http://www.idealibrary.com on IDEAL®

Sintering of Nickel Steam-Reforming Catalysts on $MgAl_2O_4$ Spinel Supports

J. Sehested,*,[1] A. Carlsson,* T. V. W. Janssens,* P. L. Hansen,* and A. K. Datye†,[1]

*Haldor Topsøe A/S, Nymøllevej 55, Lyngby DK-2800, Denmark; and †Department of Chemical & Nuclear Engineering, University of New Mexico, Albuquerque, New Mexico 87131

Received July 13, 2000; revised September 26, 2000; accepted September 26, 2000

Sintering significantly contributes to the deactivation of Ni-based steam-reforming catalysts. We have investigated the effect of Ni loading and surface area of the support on sintering of Ni particles on $MgAl_2O_4$ spinel supports. The experiments were performed under simulated industrial pre-reforming conditions, i.e., in a 10 : 1 mixture of steam and hydrogen at 500°C and 30 bar total pressure. The Ni particle size of fresh and sintered catalysts was determined from sulfur chemisorption capacity, X-ray diffraction (XRD), transmission electron microscopy (TEM), and scanning transmission electron microscopy (STEM). It was found that most of the sintering occurs in the first 200 h; after that period the Ni particle size changes only slightly. A remarkable result is that the average Ni particle size after sintering reaches a limiting value that depends only weakly on the Ni loading and surface area of the support. Sintering of the catalysts with a lower Ni loading is slower and they exhibit a greater loss in Ni surface area compared to those with a higher Ni loading. Because the sintered particles are polycrystalline agglomerates, the XRD estimates of particle size are lower than those obtained by the other techniques such as TEM or chemisorption. The particle size distributions derived from TEM and STEM follow a log normal distribution, suggesting that sintering occurs through crystallite migration and coalescence. The limiting size of the Ni particles after sintering, and the low sintering rate after 200 h, can both be related to the lower mobility of the larger Ni particles on the support.

Key Words: **steam reforming; nickel catalyst; sintering; particle migration; TEM; STEM.**

1. INTRODUCTION

Steam reforming is an industrial process to convert hydrocarbons with steam into mixtures of hydrogen, carbon monoxide, carbon dioxide, and methane:

$$C_nH_m + nH_2O \rightarrow nCO + (n + m/2)H_2$$
$$CO + H_2O \rightleftharpoons CO_2 + H_2.$$

Modern steam-reforming units consist of a primary reformer with a pre-reformer upstream, which reduces the load of the primary reformer, and minimizes the risk of sulfur poisoning. The operational conditions in the primary reformer are 30 bar total pressure, oxygen-to-carbon ratio of approximately 4, and a temperature between 500 and 950°C. The pre-reformer is operated adiabatically at approximately 500°C and 30 bar total pressure. In both the primary reformer and the pre-reformer, Ni-based catalysts are commonly used (1).

Sintering is an important route for the deactivation of Ni-based steam-reforming catalysts. A good understanding of the sintering mechanisms is crucial, both to predict the extent of deactivation by sintering, and to design catalysts that maintain a high activity. Several studies on the sintering of Ni particles have been reported in the literature (1–8). Sintering is a complex process, which is influenced by many parameters such as temperature, chemical environment, catalyst composition and structure, and support morphology. The most important parameters are the sintering temperature and the atmosphere over the catalyst (1–8). Increasing the temperature results in a significantly faster sintering process and the presence of water greatly accelerates the sintering process (6). The effects of initial Ni particle size distributions are small, but sintering tends to be faster for narrow particle size distributions (2). The support can affect the sintering in various ways. It has been proposed that the pore structure of the support determines the final particle size of the Ni particles. However, the morphology of the support itself changes under sintering conditions as well. Moreover, phase transitions in the support and reactions between the support and active Ni particles can affect the sintering process (7).

The objective of this study is to determine how the sintering of Ni particles proceeds at the conditions applied in pre-reforming, in particular, at high steam pressures for several weeks. However, the use of a reactive gas mixture results in a situation where the active outer shell of the catalyst experiences a gas composition different from that in the interior of the catalyst pellet. Furthermore, the gas

[1] To whom correspondence should be addressed. J.S.: E-mail: JSS@topsoe.dk; Fax: +45 45272999. A.K.D.: E-mail: datye@unm.edu; Fax: +1 (505) 277-1024.

0021-9517/01 $35.00

atmosphere also changes with conversion, so the gas atmosphere will not be the same over the entire catalyst bed. This leads to a variation in sintering conditions, and results that are difficult to interpret. Therefore, we have chosen to use a nonreactive atmosphere that contains only steam and hydrogen ($H_2O/H_2 = 10$) at an industrially relevant pressure (30 bar) and temperature (500°C), which allow for good control of the sintering conditions. We recognize that our work has only addressed the effects of a high water pressure during sintering, since no organic species are present. The influence of the organic species will be the subject of future studies.

2. EXPERIMENTAL

Six experimental steam-reforming catalysts were used in the sintering experiments reported here. The catalysts were prepared on two different supports: a 24 m^2/g $MgAl_2O_4$ spinel support (22 wt% Ni) and a 75 m^2/g Zr-doped spinel support (7.6, 14.8, 24.8, 30.0, and 36.5 wt% Ni). The surface area and Ni particle sizes were measured on both the fresh catalysts, and after 211 h and 770 h of sintering—only the catalyst containing 7.6 wt% Ni was analyzed after 86 and 700 h.

The sintering experiments were performed by exposing the catalysts to a 10 : 1 mixture of steam and hydrogen at 500°C and a total pressure of 30 bar. Prior to sintering, the catalysts were activated by reduction in H_2 at 500°C for 2 h. After sintering, the catalysts were passivated overnight at 50°C in a mixture of 1% O_2 in N_2 before they were taken out of the reactor. The fresh catalysts were passivated immediately after the reduction with the same procedure.

The surface areas (BET) of the catalysts were determined by nitrogen adsorption using a Quantachrome MONOSORB apparatus. The measured values were normalized to standard temperature and pressure in accordance with the ASTM standard for single-point determination of BET surface areas (9). The surface area of the internal standard was measured daily, giving a standard deviation of less than 2.5%.

The Ni particle sizes were determined from X-ray powder diffraction (XRD), sulfur chemisorption capacity (Scap), transmission electron microscopy (TEM), and scanning transmission electron microscopy (STEM). The XRD measurements were performed by using Cu $K\alpha$ radiation and a Philips PW1820 goniometer with Bragg–Brentano geometry. A volume-averaged Ni crystallite size is then obtained from the line broadening of the Ni(200) diffraction line using the Scherrer equation.

The sulfur chemisorption capacity gives the specific Ni surface area, from which a surface-averaged Ni particle diameter can be derived. The sulfur chemisorption was performed according to (1) using a flow of H_2S/H_2 over the catalyst until saturation. The sulfur uptake of the catalysts, in micrograms of sulfur per gram of catalyst (ppm), is then determined by oxidation of the chemisorbed sulfur at high temperature, measuring the amount of SO_2 that comes off by infrared detection. Under the experimental conditions given in (1), the specific Ni surface area can be calculated from the sulfur capacity from the relationship that 440 ppm S is equivalent to 1 m^2/g Ni (1, 10). Finally, this can be converted to a surface-averaged nickel particle diameter, given by (1)

$$d_{\mathrm{Scap}} = 3000\frac{X_{\mathrm{Ni}}}{S}, \qquad [1]$$

where d_{Scap} is the diameter of the Ni particles in nanometers, X_{Ni} is the Ni loading in weight percent, and S is the sulfur capacity in parts per million.

TEM and STEM images directly yield the size and shape of the Ni particles. Both the TEM and STEM measurements were done on a Philips CM200 FEG electron microscope, which has a primary electron energy of 200 keV and a point resolution of 1.9 Å in TEM mode. The resolution in STEM depends, of course, on the spot size used; in the experiments here, the resolution is about 1 nm, which implies that atomic details cannot be observed. For the microscopy experiments, air-exposed, passivated catalyst pellets were crushed to a fine powder, dispersed in ethanol, and deposited on a Cu TEM grid with a holey carbon film.

The advantage of electron microscopy is that complete particle size distributions can be obtained. From the particle size distributions, both the surface-averaged and volume-averaged particle sizes can be calculated, which then can be compared to the values obtained with the sizes obtained from sulfur chemisorption capacity and XRD measurements, respectively. The surface-averaged diameter d_s is given by

$$d_s = \frac{\sum n_i d_i^3}{\sum n_i d_i^2}, \qquad [2]$$

where n_i is the number of particles with a diameter d_i. The particles were all treated as spherical; deviations from spherical geometry were accounted for by using an average diameter. Likewise, the volume-averaged diameter d_v can be written as

$$d_v = \frac{\sum n_i d_i^4}{\sum n_i d_i^3}, \qquad [3]$$

with the same definitions of the symbols as used in Eq. [2].

3. RESULTS

The progress of sintering, as measured by the BET surface area, is shown in Fig. 1; the corresponding values are given in Table 1. The reduction in surface area is about 40% for the catalysts with the highest surface area, and about 20% for the catalyst with the lowest surface area. Both the Ni and spinel support contribute to the decrease

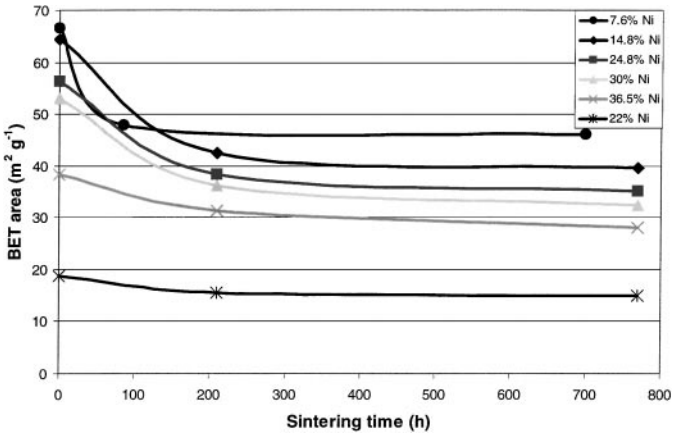

FIG. 1. BET surface area plotted as a function of sintering time.

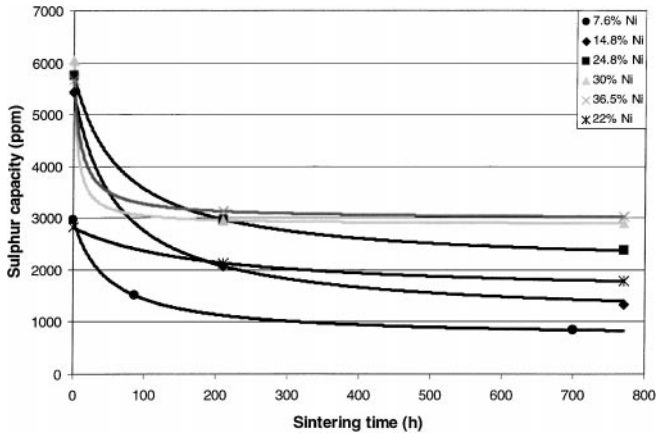

FIG. 2. Sulfur capacity plotted as a function of sintering time.

in BET surface area. For all catalysts, most of the loss in surface area occurs quite rapidly—within the first 211 h of sintering; after that, the process becomes much slower. Since a reduction in the measured surface area might as well be caused by obstructions in the pore system, the pore volume of the catalyst with 36.5 wt% Ni was determined before and after sintering by mercury porosimetry. No loss in pore volume was measured after sintering, and therefore it was concluded that pore blockage is not important. Consequently, the loss in surface area is completely assigned to sintering.

The decrease in sulfur adsorption capacity, shown in Fig. 2, follows the same trend as the BET surface area; the corresponding Ni surface areas per gram of catalyst are listed in Table 2. The sulfur capacities are the same for crushed catalysts and pellets, which indicates that pore blockage is insignificant. Pore blockage, if present, would have resulted in a higher sulfur capacity for the crushed catalysts. The Ni surface area of the catalyst with 22% Ni is reduced by approximately 25% in the first 211 h and by another 10% after that. The other catalysts lose about 50–60% of their nickel surface area in the first 211 h; the additional loss between 211 and 770 h varies from 0 to approximately 25%, and increases with decreasing Ni loading. An attempt was made to quantify this effect by fitting the data to a second-order generalized power law expression (GPLE), which works well for most systems (6, 11),

$$\frac{d}{dt}\left(\frac{S}{S_0}\right) = k_2\left(\frac{S - S_{eq}}{S_0}\right)^2, \qquad [4]$$

where S is the sulfur chemisorption capacity as a function of time, S_0 is the sulfur capacity of the fresh catalyst, S_{eq} is the final sulfur capacity after sintering for long times, and k_2 is the second-order decay rate constant. With this equation, we can find values for the rate constants k_2, and a final sulfur chemisorption capacity S_{eq}, which can be converted to a final Ni surface area; these are also listed in Table 2. Although the values are quite uncertain due to the limited number of data points, k_2 is clearly higher for the catalysts with 30.0 and 36.5 wt% Ni, indicating that catalysts with a high Ni loading reach their equilibrium state faster than the other catalysts.

The Ni surface areas found from the sulfur chemisorption capacity measurements can be converted to Ni particle diameters by using Eq. [1]. These diameters for the fresh and

TABLE 1

BET Surface Areas for Fresh and Sintered $Ni/MgAl_2O_4$ Spinel Catalysts

Sintering time	7.6% Ni/spinel (m^2/g cat.)	14.8% Ni/spinel (m^2/g cat.)	24.8% Ni/spinel (m^2/g cat.)	30% Ni/spinel (m^2/g cat.)	36.5% Ni/spinel (m^2/g cat.)	22% Ni/spinel (m^2/g cat.)
Fresh	66.5	64.5	56.3	53.0	43.8	18.7
211 h	47.9[a]	42.4	38.3	42.4	31.4	15.5
770 h	46.0[b]	39.6	35.1	39.6	28.1	15.0
770 h[c]	49.8[b]	46.5	46.7	50.1	44.2	19.2

[a] Sintering time, 86 h.
[b] Sintering time, 700 h.
[c] Surface area per gram of support.

TABLE 2

Specific Ni Surface Areas Derived from the Sulfur Chemisorption Capacities, Equilibrium Surface Areas (Eq. [4]), and Sintering Rate Constant of the Ni/$MgAl_2O_4$ Spinel Catalysts

Sintering time	7.6% Ni/spinel	14.8% Ni/spinel	24.8% Ni/spinel	30% Ni/spinel	36.5% Ni/spinel	22% Ni/spinel
Fresh (m^2/g)	6.7	12.3	13.1	13.7	12.9	6.4
211 h (m^2/g)	3.4[a]	4.7	6.8	6.7	7.1	4.8
770 h (m^2/g)	1.9[b]	3.2	5.4	6.6	6.9	4.0
Equilibrium[c] (m^2/g)	1.6	2.5	4.7	6.5	6.8	3.6
Percent loss	76%	80%	64%	52%	47%	44%
$k_2 \times 10^2$ $(h)^{-1}$	2.27	1.97	2.27	32.8	17.0	1.20

[a] Sintering time, 86 h.
[b] Sintering time, 700 h.
[c] S_{eq} from the GPLE fit to the data.

sintered catalysts are given in Table 3. In addition, the diameters determined from the final sulfur capacity (S_{eq}) are listed as well. The Ni particle diameters in the fresh catalyst (on the support with higher surface area) increase with the Ni loading from 7.7 nm at 7.6 wt% Ni to 19.3 nm at 36.5 wt% Ni. After 770 h of sintering, we find that the diameter for the lower surface area catalyst (22 wt% Ni) has increased from 23.4 to 37.1 nm. Similar increases in diameter are seen for the other catalysts. Remarkably, the Ni particle diameters after 700–770 h of sintering lie in a narrow range, 27 to 37 nm for all catalysts studied here, despite an almost 5-fold variation in Ni loading. The average Ni crystallite size in the catalyst with 22 wt% Ni also falls in this range, despite the different pore structure and particle size of the support, as inferred from the BET surface area. Therefore, we conclude that the final nickel particle size after sintering depends only weakly on the Ni loading and support texture.

The Ni particle diameters derived from the Ni(200) line broadening in XRD are also included in Table 3. Generally, the diameters found from XRD are lower than those derived from the sulfur chemisorption capacity. Nevertheless, these data also indicate an increase in particle size with increasing Ni loading for the fresh catalyst, and a size that is largely independent of the Ni loading after sintering, in agreement with the data derived from the sulfur capacity measurements. The XRD data for the sintered catalyst, however, do show a higher particle size on the catalyst with the lower surface area support (22 wt% Ni).

A more direct way to determine the Ni particle sizes is to measure them in TEM and STEM images and derive particle size distributions. Figure 3 shows typical TEM (left) and STEM (right) images of the sintered catalyst. With conventional TEM, the Ni particles are sometimes difficult to distinguish from the spinel support, since they have similar size and contrast. By changing to STEM mode with a

TABLE 3

Nickel Crystallite Diameters (nm)

Sintering time	Analysis method	7.6% Ni/spinel	14.8% Ni/spinel	24.8% Ni/spinel	30% Ni/spinel	36.5% Ni/spinel	22% Ni/spinel
0 h	XRD	Peak too small	5.5	5.6	8.3	12.0	12.0
	TEM (d_v)		7.2	—	—	—	13.9
	TEM (d_s)		6.6	—	—	—	11.1
	Chemisorption[a]	7.7	8.2	12.9	14.9	19.3	23.4
770 h	XRD	12.0[b]	14.0	12.5	12.0	14.0	24.0
	TEM (d_v)	20.5[b]	33.0	—	—	45.7	34.1
	TEM (d_s)	17.7[b]	29.9	—	—	37.8	28.8
	Chemisorption[a]	27.0	31.7	31.4	31.0	36.2	37.1
Equilibrium[c]	d_{final}	32.7	41.5	36.0	31.3	36.7	41.5

[a] D_{Scap} as derived from the sulfur adsorption capacity.
[b] Sintering time, 700 h.
[c] Equilibrium diameter after sintering for long times (from Eq. [4]) based on S_{eq}.

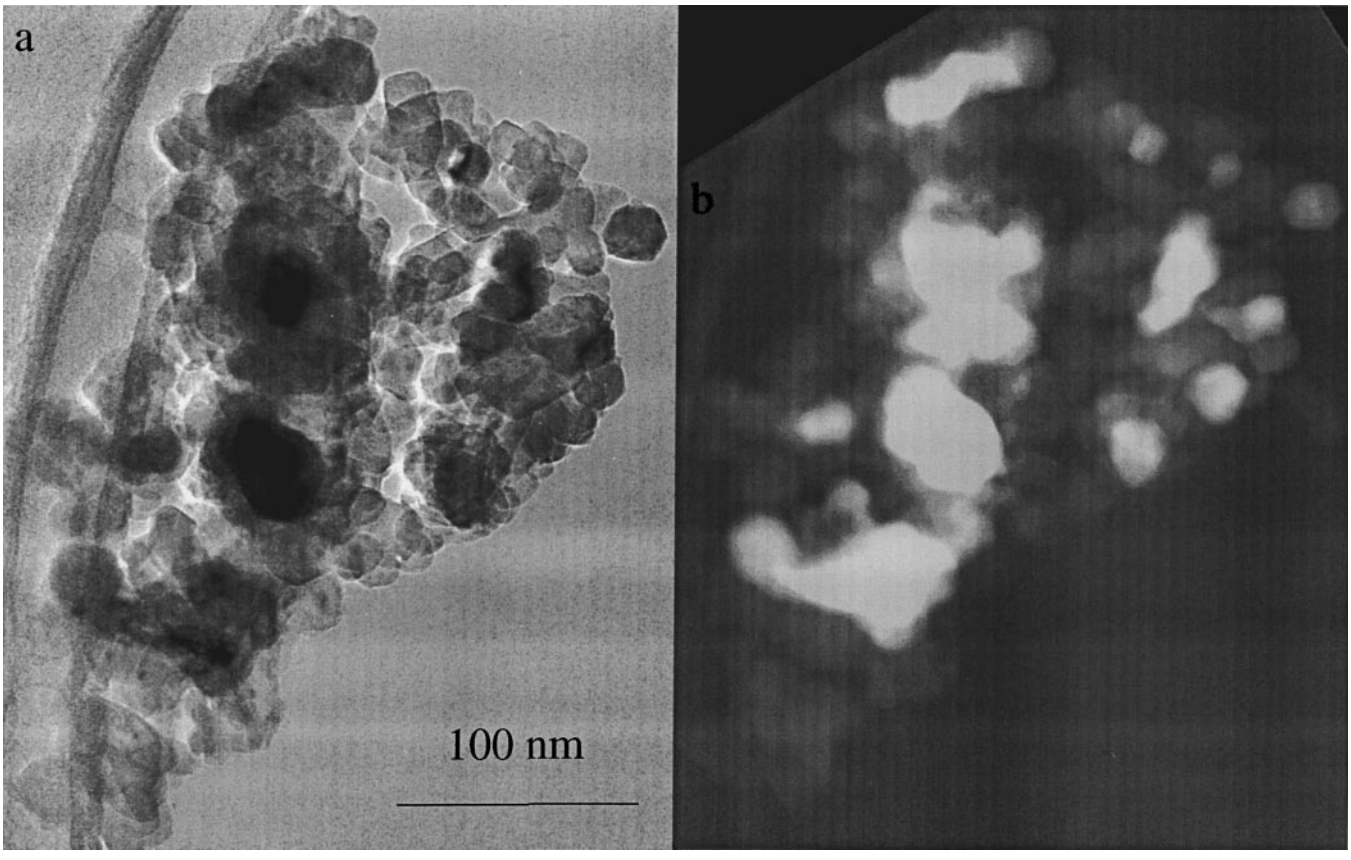

FIG. 3. Low-magnification view of 15 wt% Ni/HSA spinel after sintering for 770 h. (a) BF TEM and (b) HAADF STEM image.

high-angle annular dark field (HAADF) detector, excellent contrast between the Ni particles and support is obtained (see Fig. 3): the Ni particles appear white in the images, while the spinel particles remain dark.

Figure 4 shows the Ni particle size distributions for the fresh and sintered catalysts with 14.8 (left) and 22 wt% Ni (right). The distributions for the fresh catalysts were derived from TEM images, while those of the sintered catalysts were obtained from the HAADF images. It appears that a log normal distribution gives a good description of the particle size distributions in these catalysts. Figure 5 shows the particle size distributions after 700–770 h sintering for the 7.6 wt% and 36.5% Ni catalysts. These catalysts contain the same support, but represent metal loadings that differ almost by a factor of 5. Once again, the similarity in particle size distribution is evident. The surface- and volume-averaged particle diameters derived from these distributions by application of Eqs. [2] and [3] have been included in Table 3.

4. DISCUSSION

In accordance with most other studies on sintering of Ni catalysts, we have found that the major part of the sintering occurs early (during the first 200 h, in our study) as indicated by both the BET and sulfur chemisorption capacity measurements in Figs. 1 and 2. The data for the catalyst with 7.6 wt% Ni show that the most significant changes occur in the first 86 h. Since no data were collected at shorter time intervals, the details of the sintering process at short times cannot be inferred from our study.

Although particle sizes derived from TEM/STEM, sulfur chemisorption, and XRD in general show the same trends, there are some discrepancies between the values found with those techniques, due to the limitations of each method. The most obvious discrepancy is the much smaller size of the sintered Ni particles found by XRD. This is an indication that the sintered Ni particles are polycrystalline: XRD gives an average size of the crystalline domains, which are smaller than the total particle size estimated by TEM and sulfur chemisorption. The presence of twin planes in the TEM pictures (see Fig. 6) of the sintered Ni particles further supports this conclusion. A similar conclusion was reached in earlier sintering studies on Ni catalysts (3, 12).

For the fresh catalysts, XRD tends to give slightly lower values than TEM, while the values found from the sulfur capacity are larger. A possible reason for this discrepancy is that XRD and TEM were performed with air-exposed, passivated catalysts, and both techniques yield the size of

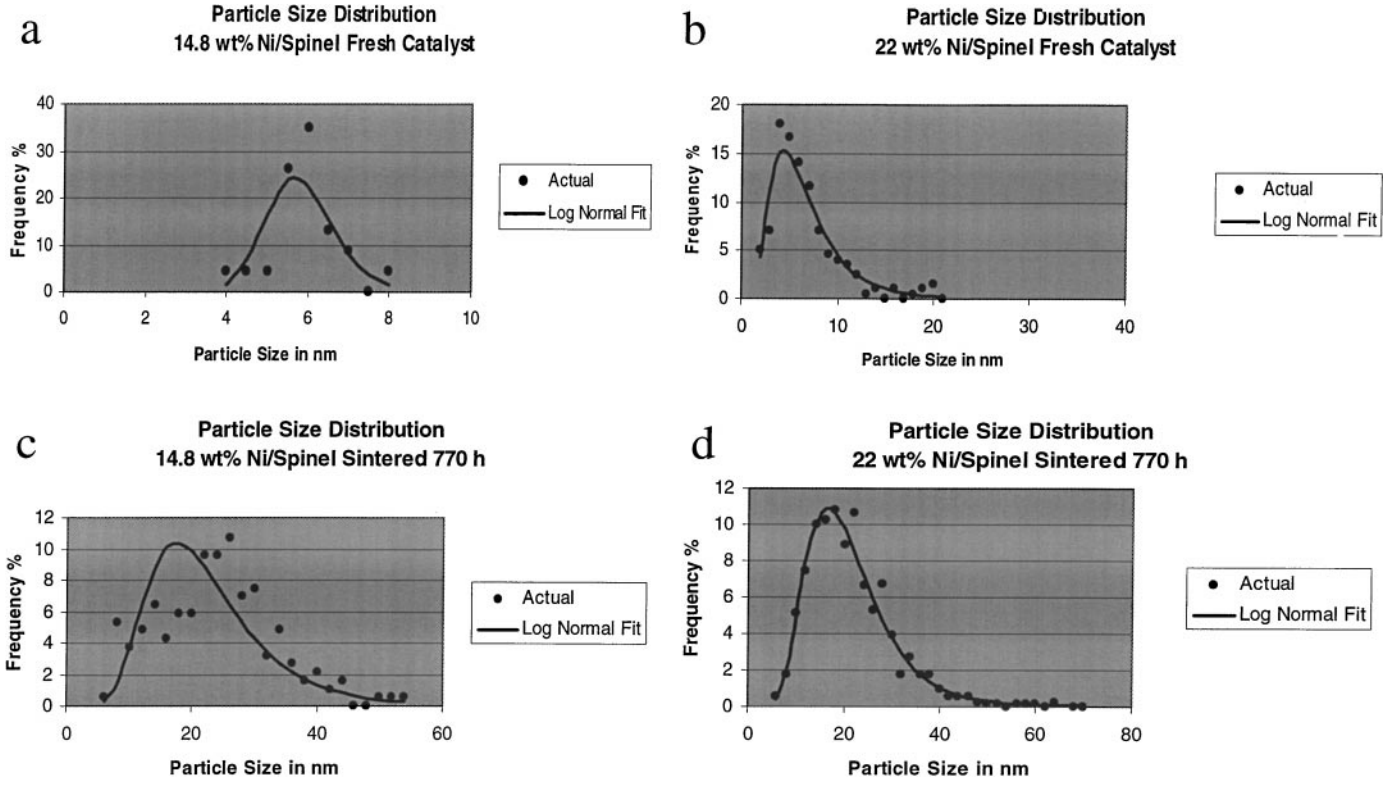

FIG. 4. Particle size distributions in sintered Ni catalysts: (a) fresh 14.8 wt% Ni/spinel (20 particles counted), (b) fresh 22 wt% Ni/spinel (199 particles counted), (c) 14.8 wt% Ni/spinel sintered for 770 h (187 particles counted), and (d) 22 wt% Ni/spinel sintered for 770 h (740 particles counted).

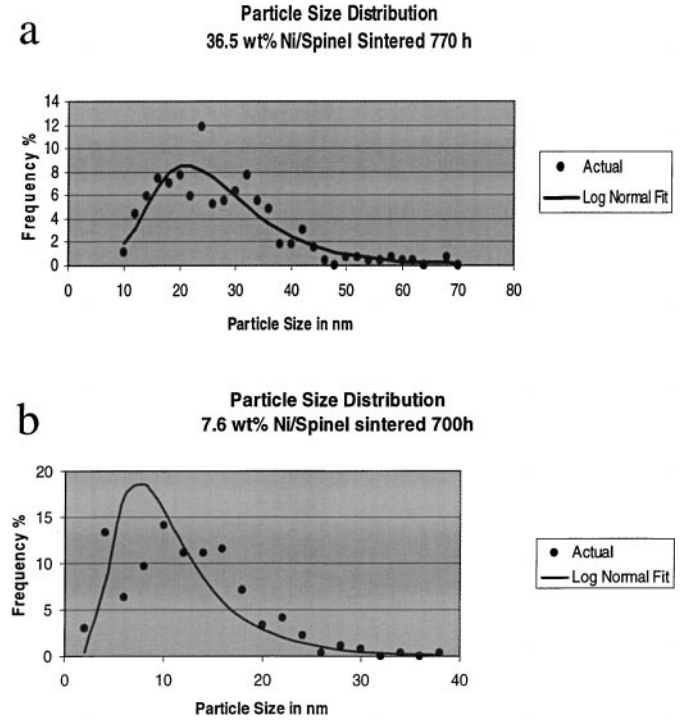

FIG. 5. Particle size distributions in sintered Ni catalysts: (a) 7.6 wt% Ni/spinel sintered for 700 h (269 particles counted) and (b) 36.5 wt% Ni/spinel sintered for 770 h (271 particles counted).

the crystalline Ni phase. Passivation causes a surface oxide layer to form on the Ni metal surface, which is not detected by XRD, causing the XRD estimate of crystallite to be too low. This is especially important for small Ni particles, where the surface oxide makes up a significant part of the particles. The passivating oxide would not affect STEM estimates of the sintered catalyst particles, which are larger and better defined.

Chemisorption, on the other hand, could overestimate the particle size, especially in the fresh catalyst. Figures 7 and 8 show TEM images of the 36.5 wt% and the 22 wt% Ni catalyst in their freshly reduced state. We see extensive contact between the Ni and the spinel support, which would lower the total uptake over what might be expected from spherical particles. Sulfur chemisorption sees only exposed Ni metal atoms; Ni atoms at the metal support interface are not considered. Depending on the extent of metal–support contact, a significant number of metal atoms may not be accessible for S chemisorption. Hence, we can expect chemisorption to overestimate average particle size in the fresh catalyst. On the other hand, for the sintered catalysts, the agreement between the average particle sizes derived from sulfur chemisorption capacities and microscopy is quite good. This might reflect the nearly spherical shapes adopted by the metal particles in the sintered catalyst (see Figs. 3 and 6).

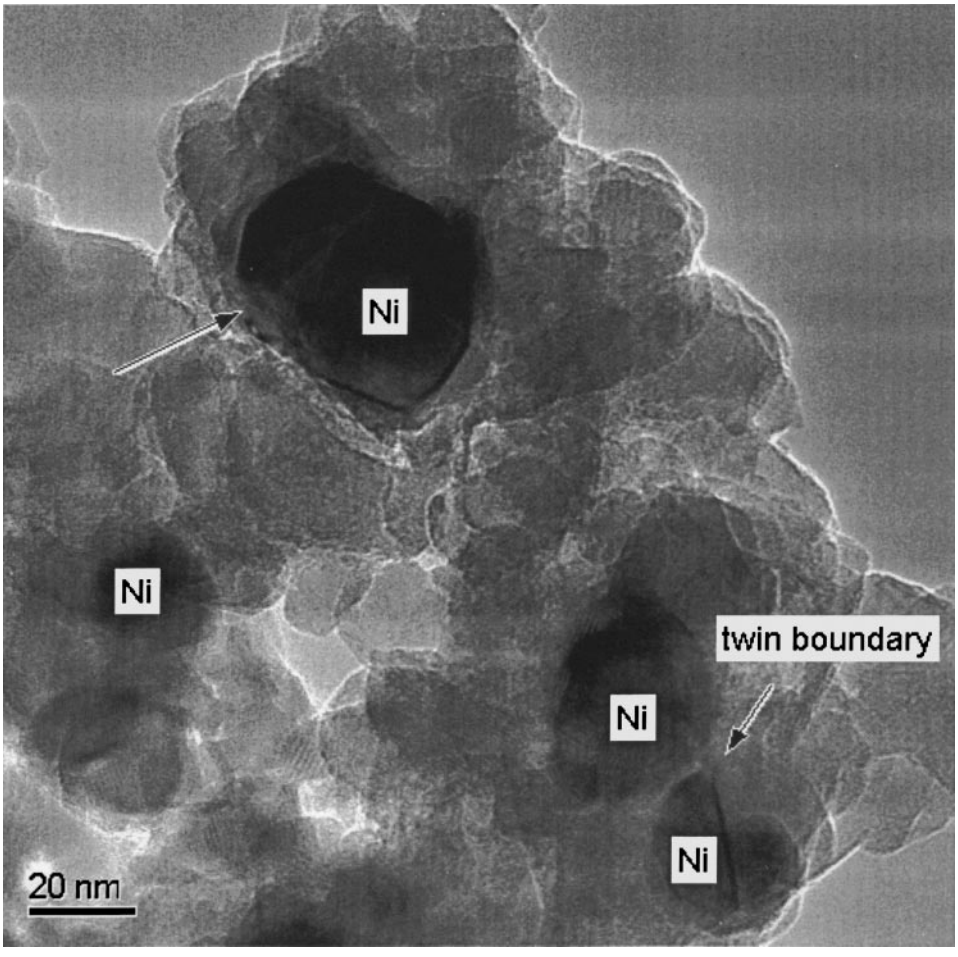

FIG. 6. Higher magnification view of the 14.8% Ni/spinel catalyst after 770 h of sintering. The arrows show the presence of internal faults in sintered Ni particles.

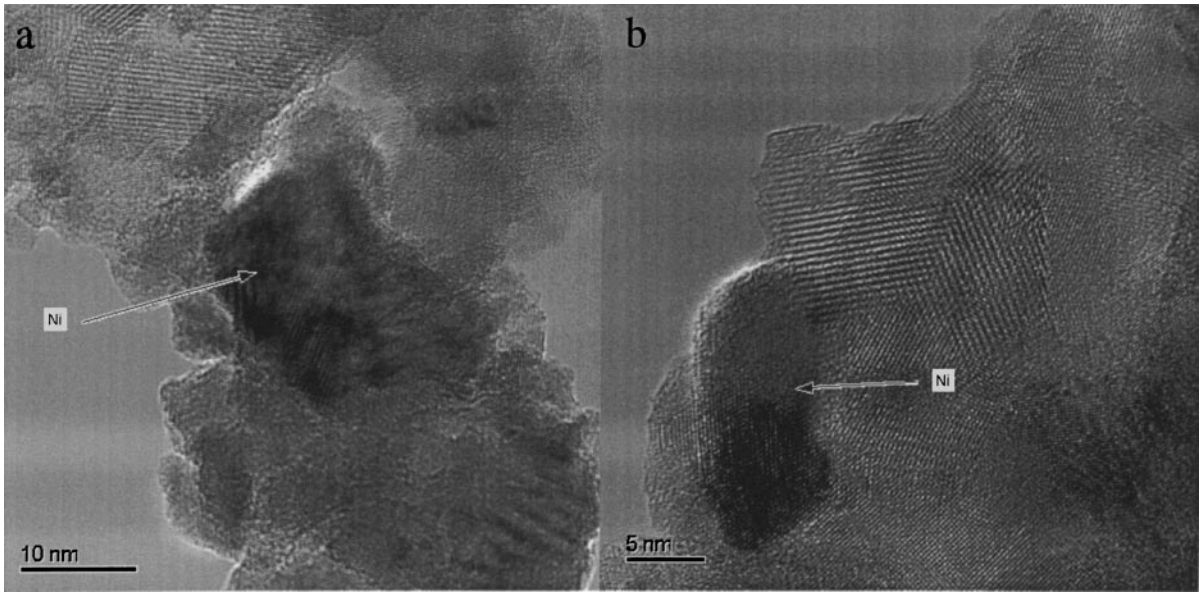

FIG. 7. TEM images of the 36.5 wt% Ni catalyst in its freshly reduced state. The images show the irregular shapes of these Ni particles and the extensive metal–support contact. The particle size distribution on this catalyst was not measured.

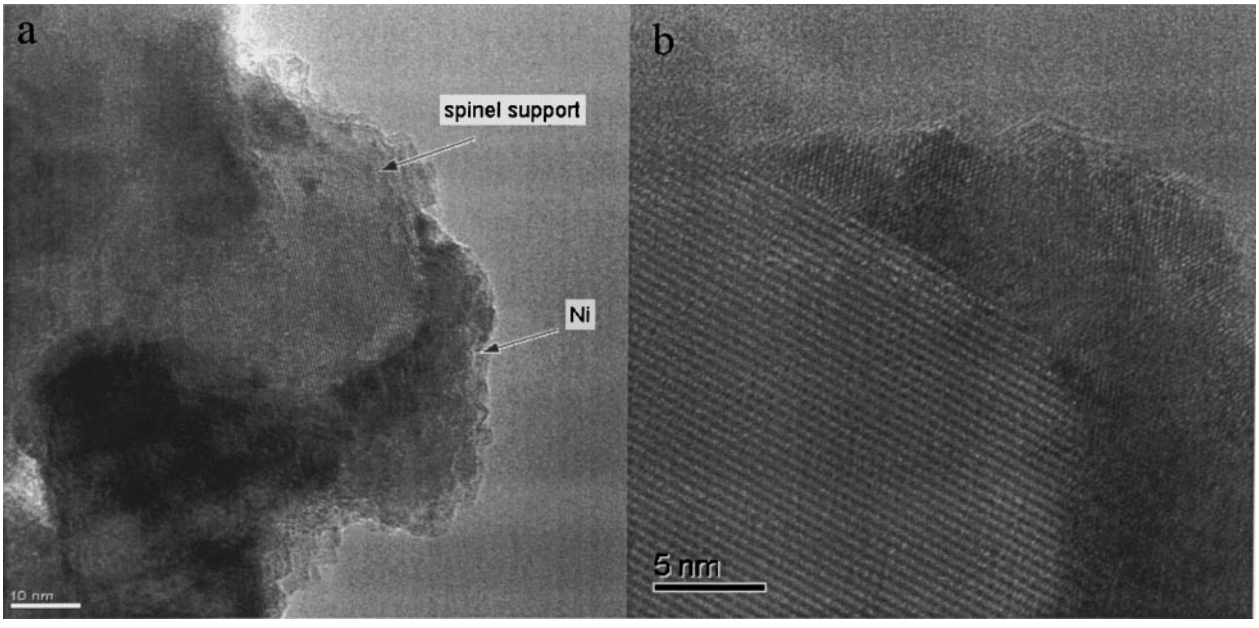

FIG. 8. TEM images of the 22 wt% Ni catalyst in its freshly reduced state. The higher magnification view on the right (b) is suggestive of the metal particle wetting the support. Such metal–support contact would make it difficult to accurately derive an average metal diameter on the basis of chemisorption.

An important parameter that was varied in this study was Ni metal loading. Since two different supports were used, the loading we should consider is the actual nickel surface loading expressed in grams of nickel per square meter of support, which is listed in Table 4. For the catalysts studied here, the Ni surface loading varies by a factor of 10 from 1.1 mg/m^2 to 12 mg/m^2. Using the Ni surface loading and the surface-averaged particle size determined by chemisorption, it is possible to estimate the number of Ni particles per square meter of support ("particle density"). This is only an estimate, since it is based on an average particle size, rather than a direct counting of all the particles. We do not have TEM data on all of the catalysts to make a statistically significant correlation; however, the observed trends from the chemisorption-averaged diameter are still informative. First we note that particle densities on the fresh catalyst show no clear trend. The catalyst preparation conditions may not be conducive to yield a controlled nucleation process. It is often thought that during sintering, the number of particles is determined by favorable anchoring sites on the support. Our data do not lend credence to such a hypothesis. We find that after sintering, the number of particles per square meter increases monotonically with metal loading. A linear increase in the number of particles per square meter with increasing metal loading would be consistent with a particle size that is invariant with loading. The correlation is not perfect, since a 5-fold variation in particle number density results from a 10-fold variation in loading. The less than perfect correlation between metal particle density and metal loading may be explained as follows: the lower-weight loading catalysts have not reached their limiting size, while the higher-loaded catalysts have reached their stable, equilibrium size distribution. This causes the range of particle densities to be smaller than would be expected at equilibrium. Our results therefore support the conclusion that the Ni particles reach a limiting size, after sintering for long times.

TABLE 4

Ni Surface Loading and Particle Densities (per Square Meter of Support Surface Area) for Fresh and Sintered Ni Catalysts, Derived from Sulfur Chemisorption Capacity

Catalyst	Ni surface loading (mg/m^2 support)	Particle Density ($\times 10^{14}$ m^{-2} support)	
		Fresh	Sintered
7.6% Ni/spinel	1.1	5.2	0.18[a]
14.8% Ni/spinel	2.3	9.1	0.24
24.8% Ni/spinel	4.4	4.4	0.47
30.0% Ni/spinel	5.7	3.7	0.62
36.5% Ni/spinel	7.7	2.3	0.53
22% Ni/spinel	11.8	1.9	0.73

[a] Sintering time, 700 h; all others 770 h.

5. FACTORS LIMITING THE GROWTH OF NI PARTICLES

A model for sintering of the Ni particles must be consistent with the three main observations in this study. The first, and perhaps the most remarkable, result is that the Ni

particle sizes after sintering depend only weakly on Ni loading, or on the surface area of the supports (see Table 3). Second, sintering is initially quite fast, but slows down significantly at long times (see Figs. 1 and 2). Third, the catalysts with a high Ni loading (30.0 and 36.5%) reach their stable state much faster than the catalysts with lower Ni loading (see Table 2).

In the literature it is suggested (1, 4) that the pore size of the support limits the size of the metal particles in a sintered catalyst, which would explain the similar particle sizes in the sintered catalysts. However, a closer examination of the TEM images of the sintered catalyst does not reveal any well-defined pores that can limit the sizes of the metal particles. The support particles themselves are not porous and the pores are the voids between the particles. Wynblatt and Gjostein (13) suggest that metal particles on concave regions of a support are more stable toward sintering than those on a convex region. The Ni particles are preferably located in the concave regions of the support, because they make contact with several support particles. The size of such concave regions, and, consequently, that of the sintered Ni particles, would then be determined by the particle size of the support. One would therefore expect the catalysts with higher support surface area to be more resistant to sintering, since the particles of the support are smaller. The support particle size in our catalysts, determined by XRD and electron microscopy, is ca. 20 nm, except for the catalyst with 22% Ni, which has a spinel particle size of ca. 60 nm. As the final Ni particle size is nearly independent of the surface area of the carrier, the final nickel diameter does not seem to be limited by primary support particle size, and hence the effective pore diameter.

To describe the sintering of metal particles, two mechanisms are generally proposed: atom migration (Ostwald ripening) and crystallite migration (coalescence). Ostwald ripening refers to the process whereby metal atoms are emitted from one metal particle and captured by another metal particle. The driving force for this process is the difference in surface energy, which varies inversely with particle size. In the coalescence process, the crystallites themselves move over the support and collide to form larger particles. In both of these processes sintering slows down with time, and results in a stable state, with a characteristic asymptotic particle size distribution.

A way to distinguish between these two models is to look at the particle size distribution after sintering. Granqvist and Buhrman (14, 15) have shown that Ostwald ripening results in a particle size distribution with a tail toward small particle sizes and a steep slope toward larger particle sizes. A recent computer simulation (16) confirms these characteristics of the size distribution from Ostwald ripening. The particle size distribution resulting from the coalescence model is a log normal distribution, which has the tail toward the large particle side, and falls steeply toward the small particle side. We find that our size distributions possess the features for a coalescence-driven sintering: a pronounced tail toward the larger particle sizes and a good fit to the log normal distribution (see Figs. 4 and 5). We therefore conclude that sintering of these Ni catalysts occurs through coalescence of particles.

The use of particle size distributions to deduce the sintering mechanism was challenged by Wanke (17), who proposed that the particle size distribution in a sintered catalyst depends on the initial distribution in the fresh catalyst, which is, in turn, determined by the method of preparation and catalyst pretreatment. A catalyst that starts off with a log normal distribution will retain a log normal distribution for short sintering times. Catalysts with different initial distributions (for example, those with bimodal distributions) will never result in a log normal distribution according to this model. While Wanke's (17) argument does have its merit, it is useful to consider the assumptions made by Granqvist and Buhrman (15) in their derivation of their statistical model for coalescence of islands: they assume that islands have undergone many collisions and it is only after a large number of such collisions that the distribution approaches a log normal distribution. If we examine the data on Ni catalysts reported since the publication of the paper by Granqvist and Buhrman (15), it appears that the log normal distribution does indeed provide a satisfactory fit in many cases. For example, Richardson and Crump (2) and Kuo *et al.* (4) found a log normal distribution on a Ni/SiO_2 coprecipitated catalyst.

The major observations in this study can be explained in terms of the coalescence model. That the limiting Ni particle size is relatively independent of the Ni loading is a consequence of the reduced mobility of larger Ni particles. This can be expressed in a particle diffusivity (D_p) for spherical particles,

$$D_p = 0.301 D_s \left(\frac{a}{R}\right)^4, \qquad [5]$$

where D_s is the surface diffusion coefficient in square centimeters per second, a is the atomic diameter, which for Ni is 0.23 nm, and R is the radius of the particle. The average distance (X_p) a particle travels is given by

$$X_p = 2\sqrt{D_p t}, \qquad [6]$$

where t is time. In the overall expression, X_p becomes inversely proportional to R^2: particle migration is much faster for small particles. The diffusion coefficient at 500°C can be estimated as $D_s = 3.3 \times 10^{-14}$ cm^2/s (2). From this, it can be calculated that a Ni particle of 10 nm travels on average approximately 230 nm in 5 h. For a particle with a diameter of 30 nm, this distance is reduced to approximately 25 nm. This clearly indicates that the probability for two big particles to collide becomes very small, and a stable situation develops

as particles grow. In addition, faceting reduces the mobility of the nickel particles even more (2). The microscopy pictures clearly show that some of the Ni particles are faceted, indicating an even higher stability with respect to sintering. As the mobility and faceting are (nearly) independent of the surface area of the support and the Ni loading, this explains why the Ni particle size after sintering is similar in all catalysts studied here. The reduced mobility of the large Ni particles is also the reason why the sintering process slows down after some time.

The third result to be explained is that the catalysts with a higher Ni loading (30.0 and 36.5 wt% Ni) reach their stable state faster than those with a low Ni loading, which is reflected in the higher values for k_2 in Table 2. We should note that the rate constant k_2 derived from the power law fit (Eq. [4]) is an indication of how fast one reaches the stable state from a fresh catalyst, rather than a measure of the absolute rate of sintering. Due to the larger particles in the catalysts with higher metal loading, we would expect a lower mobility of the metal particles, and hence the drop in metal surface area to be not very pronounced. Indeed, catalysts with higher metal loading lose on average only about 50% of their initial metal surface area. On the other hand, catalysts with lower metal loading start with smaller metal particles, which have higher mobility. Hence, we would expect a greater loss in surface area for the low metal loading catalysts. Our results (Table 2) show that the loss in surface area after long-term sintering for the lower-loaded Ni catalysts is almost 80% of their initial surface area. The time needed to reach a stable surface area is a reflection of the extent of sintering the catalyst undergoes before a stable surface area is reached. Hence, it takes a much shorter time for the higher-metal-loaded catalysts to reach their stable state.

As discussed above, the three main observations in this study can be inferred from the sintering mechanism. Particle migration has also been proposed as the sintering mechanism for nickel supported on silica (2, 4). Therefore, we believe that the conclusions derived here are of general importance.

6. CONCLUSIONS

Sintering of six Ni steam-reforming catalysts was studied under conditions similar to those in an industrial prereformer, i.e., in an atmosphere of $H_2O : H_2 = 10 : 1$ at 500°C and 30 bar total pressure. Both the Ni loading and the surface area of the support were varied. Most of the sintering takes place in the first 200 h. Catalysts with a higher Ni loading reach their stable state faster than those with a lower loading. The final Ni particle sizes after sintering is limited to approximately 30 nm in our catalysts, and depends only weakly on the metal loading and the surface area of the support. Furthermore, the particle size distributions after sintering can be effectively described by a log normal distribution. This indicates that sintering of Ni particles in these catalysts is governed by particle migration and coalescence, rather than Ostwald ripening. The coalescence mechanism can also explain the similar size of the sintered Ni particles (independent of metal loading), and the rapid decrease in sintering rate with time.

ACKNOWLEDGMENTS

This work was performed, in part, during a sabbatical visit by A.K.D. to Haldor Topsøe A/S. The study of catalyst sintering at the University of New Mexico is supported by Grant CTS-9911174 from the U.S. National Science Foundation.

REFERENCES

1. Rostrup-Nielsen, J. R., *in* "Catalysis, Science and Technology" (J. R. Anderson and M. Boudart, Eds.), Vol. 5, Chap. 1. Springer-Verlag, Berlin, 1984.
2. Richardson, J. T., and Crump, J. G., *J. Catal.* **57**, 417 (1979).
3. Teixeira, A., and Giudici, R., *Chem. Eng. Sci.* **54**, 3609 (1999).
4. Kuo, H. K., Ganesan, P., and Deangelis, R. J., *J. Catal.* **64**, 303 (1980).
5. Bartholomew, C. H., and Sorensen, W. L., *J. Catal.* **81**, 131 (1983).
6. Bartholomew, C. H., *Appl. Catal. A* **107**, 1 (1993).
7. Young, D. J., Udaja, P., and Trimm, D. L., *Surf. Sci. Catal.* **6**, 331 (1980).
8. Borisova, M. S., Fenelov, V. B., Dzisko, V. A., and Simonova, L. G., *Kinet. Katal.* **17**, 653 (1976).
9. ASTM D4567, "Standard Test Method for Single-Point Determination of Specific Surface Area of Catalysts Using Nitrogen Adsorption by Continuous Flow Method."
10. Alstrup, I., Rostrup-Nielsen, J. R., and Røen, S., *Appl. Catal.* **1**, 303 (1981).
11. Fuentes, G. A., and Gamas, E. D., *in* "Catalyst Deactivation" (C. H. Bartholomew and J. B. Butt, Eds.), p. 637. Elsevier, Amsterdam, 1991.
12. Borowiecki, T., Denis, A., Nazimek, D., Grzegorczyk, W., and Barcicki, J., *Chem. Stosow.* **27**, 229 (1983).
13. Wynblatt, P., and Gjostein, N. A., *Prog. Solid State Chem.* **9**, 21 (1975).
14. Granqvist, C. G., and Buhrman, R. A., *Appl. Phys. Lett.* **27**, 693 (1975).
15. Granqvist, C. G., and Buhrman, R. A., *J. Catal.* **42**, 477 (1976).
16. De Smet, Y., Deriemaeker, L., and Finsy, R., *Langmuir* **13**, 6884 (1997).
17. Wanke, S. E., *J. Catal.* **46**, 234 (1977).